Broadband 1–3 Piezoelectric Composite Transducer Design Using Sierpinski Gasket Fractal Geometry

Haoyu Fang, *Member, IEEE*, Zhen Qiu, *Member, IEEE*, Anthony J. Mulholland, Richard L. O'Leary, *Member, IEEE*, and Anthony Gachagan, *Member, IEEE*

***Abstract*— Wider operational bandwidth is an important requirement of an ultrasound transducer across many applications. In nature, it can be observed that several hearing organs possess a broad operating bandwidth by having a varying length scales structure. Moreover, conventional 1–3 piezoelectric composite transducers have been widely recognized for their wider bandwidth over their piezoelectric ceramic counterparts. In this paper, a novel 1–3 piezoelectric composite design using a fractal geometry, known as the Sierpinski Gasket (SG), is proposed in order to explore the potential of further extending the operational bandwidth and sensitivity of the transducer. Two equivalent 1–3 piezocomposite designs are compared to this end, one with a conventional periodic parallelepiped-shaped pillar structure and one with the SG fractal geometry, both theoretically, using a finite-element analysis package, and experimentally. The transmit voltage response and open-circuit voltage response are used to illustrate bandwidth improvement from the fractal composite design. Following the simulation results, a 580-kHz single-element transducer, utilizing the proposed SG fractal microstructure, is fabricated using a pillar placement methodology. The performance of the prototyped device is characterized and compared with a conventional 1–3 composite design, as well as with a commercial ultrasound transducer. In the one-way transmission mode, a bandwidth improvement of 27.2% and sensitivity enhancement of 3.8 dB can be found with the SG fractal design compared to an equivalent conventional composite design and up 105.1% bandwidth improvement when compared to the commercial transducer. In the one-way reception mode, the bandwidth improvement for the SG fractal design is 2.5% and 32.9% when compared to the conventional and commercial transducers, respectively.**

***Index Terms*— Broadband, fractal, piezocomposite, Sierpinski gasket (SG), ultrasonic tranducer.**

I. Introduction

THE concept of a "piezoelectric composite" ultrasound transducer is well-established [1]–[3]; such ultrasound transducers comprise an active piezoelectric phase and a passive, typically polymer phase. Such piezoelectric composite configurations, when designed correctly, can attain high sensitivity while being well matched to a low acoustic impedance load [4], [5]. Piezoelectric composite ultrasound transducers with a wide operational bandwidth are preferred in many applications, such as underwater sonar, nondestructive testing, and biomedical imaging [6]–[9]. A broadband transducer can offer better spatial resolution and, therefore, better imaging performance. Wider operational bandwidth at the transducer can offer advantages in the signal processing chain of contemporary imaging systems. Frequency diverse signal processing techniques such as split spectrum processing [10] benefit form wider transducers bandwidth when applied to speckle reduction [11] and contrast enhancement [7].

There are many different techniques which have been developed in order to achieve the enhancement of the operational bandwidth for an ultrasound transducer. To summarize, there are three popular methods to achieve this goal.

1) Improve the piezoelectric material properties.
2) Modify the matching/backing design.
3) Optimize the composite structure, including the filler material properties.

For enhancing the piezoelectric material properties, Yamada *et al.* [12] proposed a method of designing a broadband ultrasound transducer by giving the piezoelectric plate a temperature gradient in its thickness direction via a controlled temperature-based depoling procedure, resulting in a graded piezoelectric constant (e_{33}) [12]. Wong *et al.* [13] designed a high-frequency phased-array ultrasound transducer with a $Pb(Mg_{1/3}Nb_{2/3})O_3 - PbTiO_3$ (PMN-PT) single crystal material and when compared with other piezoceramic designs, this single crystal material exhibited a wider operational bandwidth. For increasing the transducer bandwidth with an optimized matching design, Hossack and Auld [14] reported a novel transducer design with an active piezoelectric matching layer. Moreover, many researchers improved the bandwidth of the ultrasound transducer by optimizing the structure of the composite design. Harvey *et al.* [15] designed a random composite transducer with piezoelectric fibers to improve the device bandwidth. Ramadas *et al.* [16] developed a wideband annular piezoelectric transducer by combining four concentric piezoelectric composite annuli each exhibiting a different fundamental thickness mode resonance. Similarly, Banks *et al.* [17] proposed two novel piezoelectric composite

Manuscript received June 15, 2018; accepted October 2, 2018. Date of publication October 8, 2018; date of current version December 20, 2018. The work of H. Fang was supported by the University of Strathclyde. This work was supported by U.K. Research Center for NDE under EPSRC Grant EP/L022125/1. *(Corresponding author: Haoyu Fang.)*

H. Fang, Z. Qiu, R. L. O'Leary, and A. Gachagan are with the Centre for Ultrasonic Engineering, Electronic and Electrical Engineering Department, University of Strathclyde, Glasgow G1 1XW, U.K. (e-mail: haoyu.fang@strath.ac.uk; zhen.qiu@strath.ac.uk; richard.o-leary@strath.ac.uk; a.gachagan@strath.ac.uk).

A. J. Mulholland is with the Department of Mathematics and Statistics, University of Strathclyde, Glasgow G1 1XH, U.K. (e-mail: anthony.mulholland@strath.ac.uk).

Digital Object Identifier 10.1109/TUFFC.2018.2874384

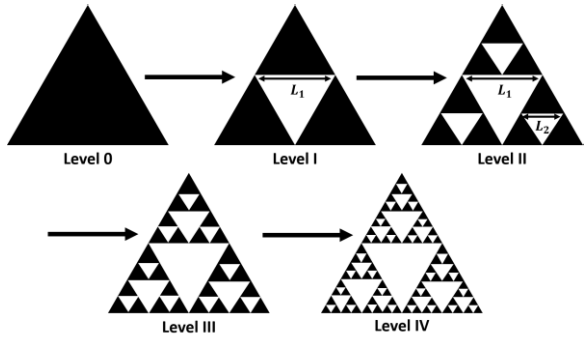

Fig. 1. First four fractal generation levels of the SG fractal geometry.

transducer designs to enhance the operating frequency of the device for air-coupled nondestructive evaluation, the dual thickness piezocomposite and conical piezocomposite design. Both designs achieved a bandwidth enhancement successfully by having a varied thickness dimension to introduce multiple thickness mode resonances into one piezocomposite design. de Espinosa *et al.* [18] developed a dual frequency 1–3 piezocomposite transducer for the purpose of performing the harmonic imaging in the field of medical ultrasound. This 1–3 piezocomposite transducer design was comprised ceramic pillars in three different shapes. By carefully choosing the thickness and different lateral dimensions of the pillars in the piezocomposite plate, two main resonance modes f and $2f$ can be obtained, which was used as the transmission mode frequency and the reception mode frequency, respectively. Guo *et al.* [19] presented a partial piezoelectric composite device design, where the thickness dimension piezoelectric plate was only partially diced and subsequently filled. The device in effect comprised a monolithic piezoelectric device combined with a piezoelectric composite. By doing so, a device exhibiting graded piezoelectric properties in the thickness direction was obtained that offered improved bandwidth at the fundamental thickness mode [19]. Yang *et al.* [20] developed a pseudorandom composite transducer by dicing the ceramic plate with two sets of cross cuts at different angles relative to the horizontal. The pulse-echo response bandwidth of this pseudorandom composite was increased by 13% when compared to a standard 1–3 composite design. These techniques support the concept that the bandwidth of an ultrasound transducer can be extended using any one of the three popular approaches described earlier.

In naturally occurring auditory systems, it is common to observe hearing organs comprised a number of different length scales. Such hearing organs exhibit extended operating bandwidth, examples include insects such as the bush cricket [21]–[23]. In common with all resonating systems, the resonance frequency of a piezoceramic resonator depends on its length scale. Therefore, having a high level of geometric complexity with a range of length results in a range of resonance frequencies, and therefore, a broadening of the overall operational frequency range.

In this paper, a self-similar fractal geometry known as the Sierpinski gasket (SG), shown in Fig. 1, will be adopted as the structure of a piezocomposite design in order to explore improvements in the bandwidth of the 1–3 composite configuration transducer. This concept of engineered transducers comprised multiple length scales has been developed mathematically [24]–[26], and these analytical models indicate that by having elements with varying length scales in the piezoelectric transducer design, the device may possess a wider operational bandwidth or a higher sensitivity compared to a conventional device. In addition, it has been shown that devices comprising triangular pillars, resulting in the absence of parallel faces between elements in a composite design, reduce the interpillar resonant activity in the lateral dimension [27]. Therefore, the thickness coupling efficiency can be increased, leading to a potential improvement in the device sensitivity.

II. Sierpinski Gasket Geometry

The primary shape of the SG fractal geometry is an equilateral triangle, where the fractal configuration at higher generation levels can be achieved by subdividing the entire equilateral triangular recursively into several similar equilateral subtriangles. The lateral width of the subtriangle at the k_{th} fractal generation level L_k can be calculated in terms of the total lateral length of the entire fractal geometry L via

$$L_k = \frac{L}{2^k}. \tag{1}$$

The finite-element (FE) analysis package, PZFlex (OnScale Inc, Cupertino, CA, USA), will be used to analyze the SG design, specifically considering the transmission and reception response of an SG fractal composite and an equivalent standard composite design to provide the proof of concept for this broadband fractal composite design approach. Then, the first prototype incorporating this SG fractal composite approach will be manufactured using a pillar placement methodology.

The performance of this SG fractal device in one-way transmission mode, one-way reception mode, and two-way pulse-echo mode will be tested experimentally and compared with the conventional composite device and an unfocused commercial ultrasound device. It will be shown, theoretically and experimentally, that an encouraging bandwidth improvement can be achieved by implementing the SG fractal geometry compared to the conventional composite design which has a regular periodic structure.

III. Modeling

A. SG Fractal Composite Transmission Performance at Different Fractal Generation Levels

First of all, how the fractal generation level of an SG fractal geometry configuration would influence the transmit performance of the piezocomposite device was investigated. In order to explore the problem space, several 3-D FE models of the unmatched SG fractal composite microstructure from fractal generation level III–level VI and their corresponding equivalent conventional 1–3 composite designs were simulated using PZFlex with water load. The active and passive phase materials are determined to be PZT-5H ceramic and hardset polymer, respectively. For each SG fractal model, the lateral length of the smallest triangular was kept as 1 mm. In terms

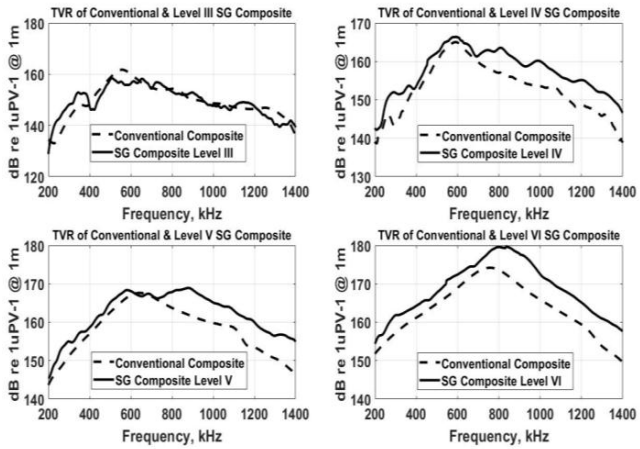

Fig. 2. Simulated TVR of the conventional and the SG composite (level III–level VI).

TABLE I
SIMULATED TVR RESULT SUMMARY FOR SG COMPOSITES FROM LEVEL III TO LEVEL VI AND EQUIVALENT CONVENTIONAL COMPOSITES

Level No.	VF	SG Composite		Conventional Composite	
		Bandwidth	Sensitivity	Bandwidth	Sensitivity
Level III	57.8 %	47.1 %	158.5 dB	35.2 %	161.8 dB
Level IV	68.4 %	71.4 %	166.5 dB	40.1 %	165.0 dB
Level V	76.3 %	82.8 %	168.4 dB	62.7 %	167.6 dB
Level VI	82.2 %	46.5 %	179.6 dB	45.0 %	174.2 dB

of each conventional 1–3 composite plate model, the pillar width was maintained the same as 1 mm, while the ceramic volume fraction (VF) was varied in order to keep it the same as the SG fractal composite design at different fractal generation levels, aiming to provide a fair comparison between the two designs in terms of the sensitivity level. The ceramic VF of the SG fractal generation level III–level VI composites and their equivalent conventional 1–3 composites are 57.8%, 68.4%, 76.3%, and 82.2%, respectively. To determine the composite thickness for all of these models, the maximum pillar aspect ratio (MPAR) concept reported by Hayward and Bennett [3] for 1–3 configurations was utilized to ensure a high electromechanical coupling efficiency in the thickness resonance mode for ceramic VFs above 50%. Accordingly, in the 1–3 composite case, the MPAR should be limited to 0.39, resulting in a 2.6-mm layer thickness and this thickness has been used in each model for a fair comparison between SG fractal composite and conventional 1–3 composite.

The transmit voltage response (TVR) spectrum of these SG composites from fractal generation level III–level VI was simulated and compared to the equivalent conventional composite designs—for each of case the results are shown in Fig. 2 and Table I.

It can be seen that the SG composite at the third level behaved approximately the same as the conventional composite. However, as the generation level increases

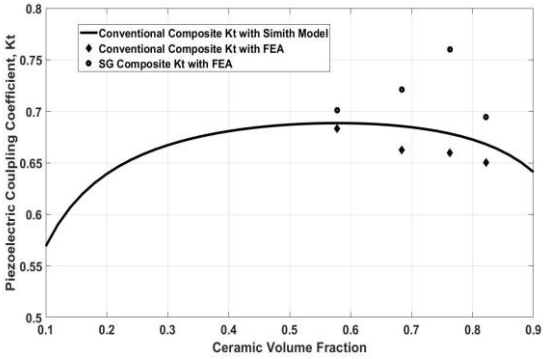

Fig. 3. Simulated k_t for SG and conventional 1–3 composite with different ceramic VFs.

beyond three, the SG composite starts to show improved fractional bandwidth when compared to the conventional composite design. For example, at generation level IV, the −6-dB bandwidth of the unmatched SG fractal composite plate is 71.4% compared to 40.1% for the conventional composite plate. Considering the difficulties of the manufacturing process, the level IV SG fractal composite was considered as a good initial choice for studying and manufacture in this work.

The effective electromechanical coupling coefficient k_t is a well understood figure of merit for transducer performance and can be calculated using (2), where it is expressed as a function of separation of the resonant frequency f_r and antiresonance f_a of the device via

$$k_t = \sqrt{\frac{\frac{\pi}{2} x \frac{f_r}{f_a}}{\tan\left(\frac{\pi}{2} x \frac{f_r}{f_a}\right)}}. \tag{2}$$

The k_t values of the four SG fractal composites and their equivalent conventional 1–3 composites were determined using the FE derived impedance spectra, these data are plotted in Fig. 3. In order to make further comparison, the k_t of the conventional 1–3 composites across the ceramic VF range was determined using the Smith–Auld model [28], again these data are plotted in Fig. 3, where it can be seen that the k_t simulated with the Smith–Auld model matches with the results achieved by the FE model for the conventional composites. In addition, the general behavior of 1–3 connectivity composites can be observed where a maximum in k_t is typically observed in the 50%–65% ceramic VF range. The motivation in the design of the 1–3 composite is to attain a maximal k_t, where in theory this is limited by the k_{33} of the piezoelectric material.

Considering the data for the SG composite devices shown in Fig. 3, k_t is observed to exhibit different behaviors to that of the conventional 1–3 composite, attaining a maximum at a higher ceramic VF than would typically be observed in a 1–3 connectivity composite. Furthermore, it can be clearly seen from Fig. 3 that the k_t of the SG composites is always higher than the equivalent conventional 1–3 composites across all the ceramic VFs under this study. Moreover, k_t of the level V SG composite is beyond the k_{33} of PZT-5H ceramic, typically 0.70. By considering (2), it can be seen that the frequency separation of the resonance and antiresonance governs the magnitude of k_t. In the SG composite device, there are number of coupled modes that act in concert at the

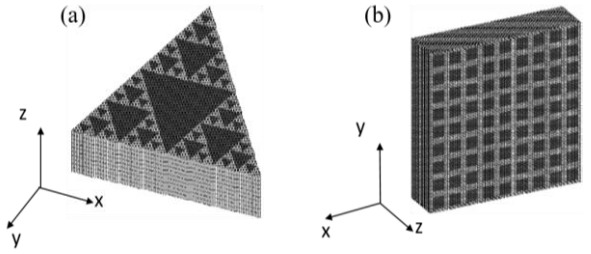

Fig. 4. Three-dimensional FE composite model. (a) Level IV SG fractal piezocomposite. (b) Conventional 1–3 piezocomposite (black: ceramic pillar and gray: polymer filler).

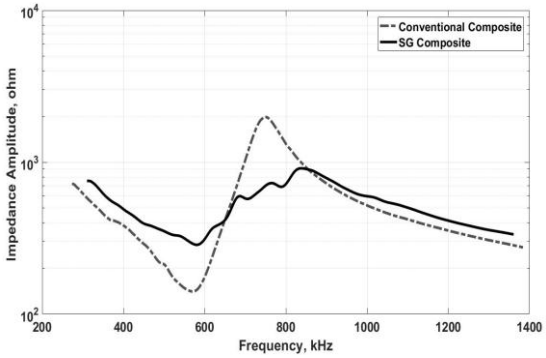

Fig. 5. FE derived electrical impedance magnitude spectrum of the SG and the conventional.

thickness mode, thereby extending the frequency separation of the two resonances resulting in a k_t for the device beyond the theoretical maximum.

In Section III-B of this paper, the SG device at level IV will undergo further analysis and its performance will be compared to a conventional 1–3 composite of the same VF. While it is recognized that a ceramic VF of 68.4% is not the optimized choice for the conventional 1–3 composite in imaging applications, although the device still gives a reasonable performance before the k_t further decreases with increased ceramic VF.

B. SG Fractal Composite at Fractal Generation Level IV

The SG fractal of generation level IV was identified for further investigation using FE modeling suit. Fig. 4(a) illustrates the SG fractal composite design, where the active phase of this SG composite is comprised equilateral triangular ceramic pillars with different lateral length scales. Fig. 4(b) shows an equivalent conventional parallelepiped 1–3 composite design. Consistency is maintained between the two composite designs in five aspects by ensuring each device has the same fundamental design parameters.

1) PZT5H ceramic and hardset polymer are chosen to be the active and passive phase, respectively.
2) The lateral length of the smallest triangular pillar at the fourth generation level in the SG composite, L_4 as defined in (1), is chosen to be 1 mm and this the same pillar width value is assigned to the conventional composite design. The kerf width of the conventional composite is 0.2 mm. The thickness of both devices is set to be 2.6 mm for the purpose of minimizing the negative effect caused by the pillar vibrating in the lateral direction.
3) Ceramic VF of both composite designs is both 68.4% because of the fixed configuration layout of the SG fractal geometry.
4) The active aperture area for both composite designs is approximately the same, which is 111 mm^2.
5) The same matching layer arrangement will be incorporated into both composite designs.

1) Electrical Impedance Profile: In order to explore the resonance behavior of the SG fractal composite in detail, the electrical impedance magnitude spectra of the level IV SG composite and conventional composite are simulated in water load without matching layer. It can be seen in Fig. 5 that the SG fractal composite and the conventional composite exhibit electrical impedance minima at 580 and 575 kHz, respectively. Moreover, a multimodal characteristic is exhibited in the SG fractal design due to its varying pillar length scale.

The resonant and antiresonant frequencies of each composites were used to calculate the effective electromechanical coupling coefficient k_t. Compared to the conventional design, the SG fractal composite achieved a larger value of k_t, which is 0.72 against 0.65 for the conventional composite. Therefore, a better energy conversion and improved bandwidth may be realized by the SG fractal design. Three modes are found in the SG fractal design at 580.0, 705.4, and 790.0 kHz. At each frequency, the displacement mode shape in thickness direction was investigated and shown in Fig. 6.

The surface dilation quality factor Q_{dil}, which is used for describing the uniformity of the surface displacement, was calculated in thickness direction using (3) for each of the three resonance frequencies shown in Fig. 6 [29]

$$Q_{\text{dil}} = \frac{D_{\text{ave}}(\omega_i)}{D_{\max}(\omega_i)} \tag{3}$$

where ω_i is the radial frequency of the ith resonance mode and D_{ave} and $D_{\max}$ is the surface average and maximum displacement, respectively. The calculated result is presented in Table II.

From Fig. 6 and Table II, the strong thickness mode behavior in the pillars associated with the second-, third-, and fourth-generation levels at 580 kHz has produced the highest Q_{dil}, which is 0.72. For the resonances at 705.4 and 790 kHz, the lateral resonances from the first- and second-generation levels dominate the vibrational response and the corresponding Q_{dil} figures are 0.21 and 0.20, respectively. These dilation quality factors are lower than a conventional 1–3 composite device, which is 0.95, due to the antiphase resonance behavior present in the triangular pillars with large pillar aspect ratio in generation levels I and II, although the main thickness mode resonance vibrational response for the SG device is still considered to be sufficiently high for acceptable operational performance. It is worth noting that the design premise of the fractal geometry composite is to couple different resonance modes and hence, the design philosophy is not directly comparable to the well-known conventional 1–3 composite theory. The operational behavior of the SG composite will now be evaluated through both simulation and experimentation.

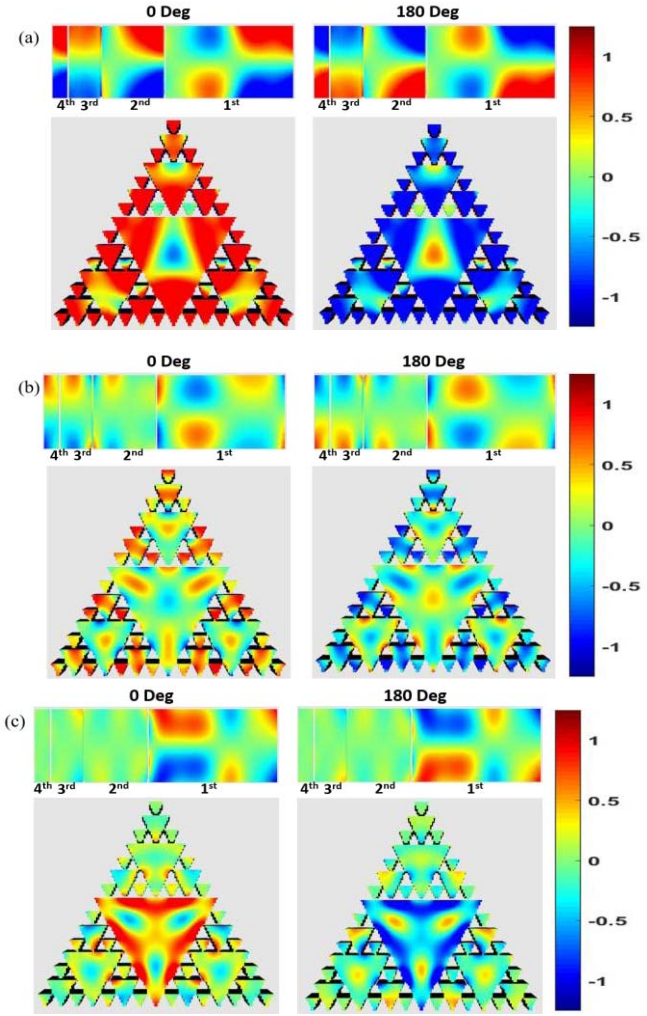

Fig. 6. SG composite displacement mode shape in thickness direction at (a) 580.0, (b) 705.4, and (c) 790.0 kHz.

TABLE II
CALCULATED Q_{dil} AT EACH RESONANCE FREQUENCIES

Resonance Frequencies	580.0 kHz	705.4 kHz	790.0 kHz
Q_{dil}	0.72	0.21	0.20

2) Pulse-Echo, Transmission, and Reception Response Modeling: In order to compare the performance of the two piezoelectric composite designs described in Section III-B, an FE model was constructed to simulate the operation of both devices when matched to a water load via a dual matching layer scheme. For the purpose of maximizing the output signal strength and to avoid obscuring the distinct resonances of the SG fractal structure, the backing layer was not incorporated into the transducer design in this paper. A schematic of the transducer arrangement is depicted in Fig. 7. The performance of the two devices, each incorporating a dual matching layer, was then assessed by considering the TVR and the open-circuit voltage (OCV) response as determined in the FE model from the simulations.

For each matching layer, the acoustic impedance Z_1 and Z_2 and thickness t_1 and t_2 can be calculated using the acoustic

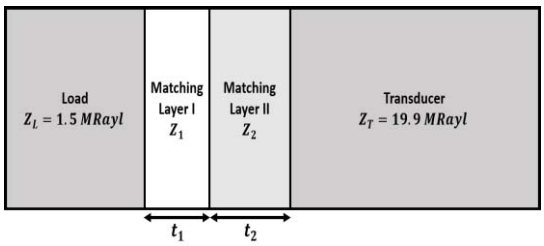

Fig. 7. Schematic of an ultrasound transducer with a dual matching layer.

impedance of the load and transducer itself, Z_L and Z_T, through the transfer matrix method [30], [31], where Z_L is 1.5 MRayl for water and Z_T is calculated using the Smith–Auld approach [28] according to the ceramic VF of the composite and material properties. As both composites have the same ceramic VF and active/passive materials, Z_T was calculated as 19.9 MRayl for both composites.

The ideal acoustic impedance of each matching layer Z_1 and Z_2 can be calculated using (4) and (5) [32]

$$Z_1 = Z_T^{\frac{1}{7}} \times Z_L^{\frac{6}{7}} \tag{4}$$

$$Z_2 = Z_T^{\frac{4}{7}} \times Z_L^{\frac{3}{7}}. \tag{5}$$

The calculated values for Z_1 and Z_2 for a theoretically optimal matching layer are 2.2 MRayl and 6.6 MRayl, respectively. Consequently, the CY221/HY956EN medium set polymer (Robnor Resin Ltd., Swindon, U.K.) was chosen as the material of the matching layer I, whose acoustic impedance is 2.68 MRayl. The RX771C(NC)/CY1300 hardset polymer (Robnor Resin Ltd., Swindon, U.K.) filled with 3-μm alumina powder using 70% weight fraction was determined to be the material of the matching layer II, which has the acoustic impedance of 6.96 MRayl [33]. Once the impedance of each layer is selected, layer thickness can be determined using (6)–(8) [30]

$$\tan\theta_1 = \alpha^{\frac{1}{2}} \left[\frac{(Z_1 - \beta Z_2)}{\beta Z_1 - Z_2}\right]^{-\frac{1}{2}} \tag{6}$$

$$\tan\theta_2 = \left[\frac{\alpha(Z_1 - \beta Z_2)}{\beta Z_1 - Z_2}\right]^{\frac{1}{2}} \tag{7}$$

where $\alpha = 4.88$, $\beta = 1.60$ (as calculated from [30]), and θ_n is the phase shift in each matching layer as determined by the wavelength λ_n and the thickness t_n of each matching layer, which is given by

$$\theta_n = 2\pi \frac{t_n}{\lambda_n}. \tag{8}$$

By using the material and equations mentioned above, at the transducers' operating frequency, 580.0 kHz, the resulting thickness of the first matching layer is 580 and 1093 μm for the second matching layer.

The predicted TVR and OCV are obtained using (9) and (10), where the resulting spectra are shown in Figs. 8 and 9, respectively. The simulated pulse-echo responses for both devices are shown in Fig. 10

$$\text{TVR} = 20\log(\text{Pressure}/V_{\text{in}}) \tag{9}$$

$$\text{OCV} = 20\log\left((V_{\text{out}}/V_{\text{in}})/(\text{Pressure}/V_{\text{in}})\right). \tag{10}$$

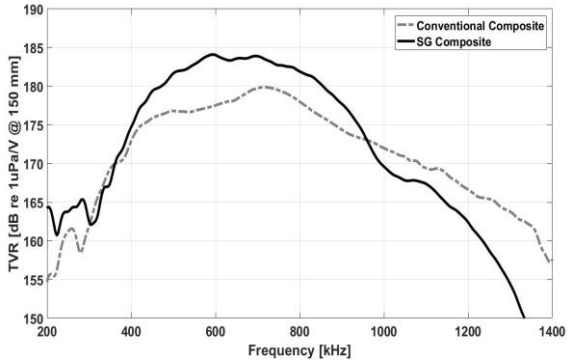

Fig. 8. Simulated TVR spectrum of the SG and the conventional composite ultrasonic transducers.

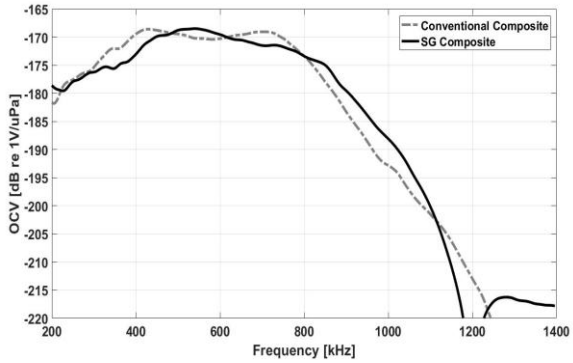

Fig. 9. Simulated OCV spectrum of the SG and the conventional composite ultrasonic transducers.

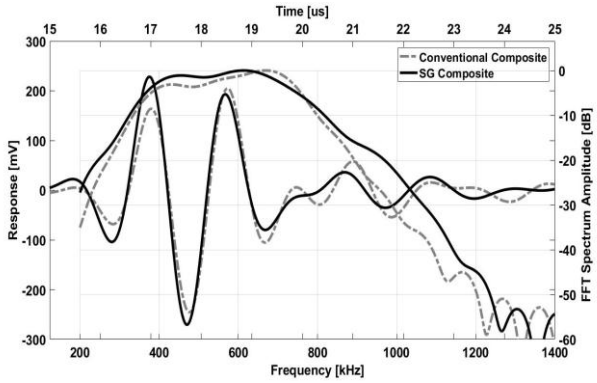

Fig. 10. Simulated pulse-echo responses of the SG and the conventional composite ultrasonic transducers.

The peak gain and −6-dB operational bandwidth for both devices in one-way transmission and reception mode and two-way pulse-echo model are shown in Table III.

As shown in Table III, by using the SG fractal geometry as the structure of a piezoelectric composite transducer design, both operational bandwidth and sensitivity level are enhanced. In transmission mode, an 8.8% bandwidth improvement and a 4.2-dB sensitivity increment were achieved. In reception mode, although the peak of the OCV of the SG fractal device and conventional device are approximately the same, the bandwidth was enhanced by 5.4% when compared to the conventional device. Finally, in the two-way pulse-echo mode, the bandwidth and signal strength improvement are 12.1% and 10.7% for the SG fractal design, when compared to the conventional composite design.

TABLE III
SIMULATED PULES-ECHO, TRANSMISSION, AND RECEPTION RESULTS

	SG Composite	Conventional Composite
Transmission Bandwidth (%)	76.9 %	70.8 %
TVR Peak (dB)	184.1 dB	179.9 dB
Reception Bandwidth (%)	85.2 %	80.8 %
OCV Peak (dB)	-168.5 dB	-168.6 dB
Pulse-Echo Bandwidth (%)	66.7 %	59.5 %
Pulse-Echo Peak-to-Peak Voltage (mV)	498.9 mV	450.8 mV

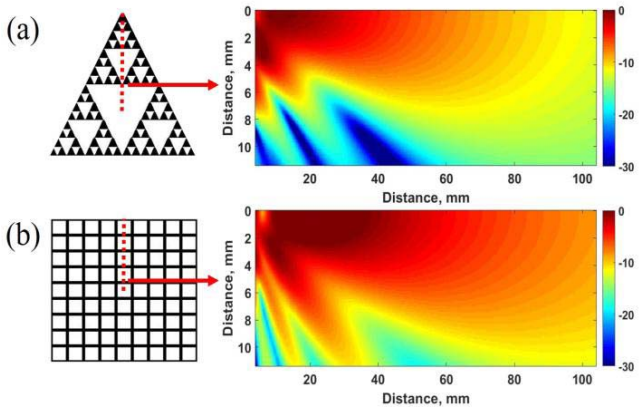

Fig. 11. Beam profile of (a) SG composite and (b) conventional composite.

3) Beam Profile Modeling: The beam profile of the SG fractal and the conventional composite at their rotating the center plane, indicated with the red dashed line in Fig. 11, was simulated using the Huygens–Fresnel principle at their resonant frequencies, which is 580 and 575 kHz, respectively.

It can be seen from Fig. 11 that the SG fractal device has a lower sidelobe level and tighter focal zone when compared to the conventional composite design. The near–far-field point of the SG fractal and the conventional composite is 9.9 and 15.6 mm, respectively, according to their different geometries.

IV. FRACTAL COMPOSITE TRANSDUCER FABRICATION

Based on the positive simulation results in Section III-B, an initial prototype SG fractal composite transducer at fractal generation level IV was manufactured. The manufacturing process of this fractal composite involved a 3-D printing technique to produce a mold, followed by a pillar placement methodology, which is described in four steps.

1) The equilateral triangular ceramic pillars at different fractal generation levels were prepared by dicing (MicroACE Series 3 Dicing Machine, Loadpoint, U.K.) commercial PZT-5H ceramic plates (Meggitt A/S, Kvistgard, Denmark) into appropriate geometries, as shown in Fig. 12(a). The lateral dimension of these

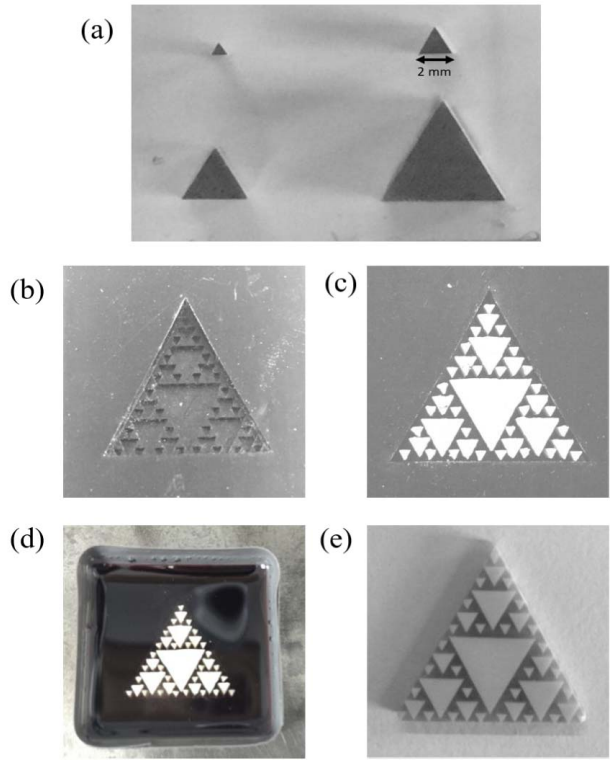

Fig. 12. SG fractal composite fabrication process (a) individual cut ceramic pillars with different sizes, (b) 3-D printed mold, (c) ceramic pillars are placed in the mold, (d) mold is filled with polymer, and (e) surplus mold is machined OFF.

equilateral triangular ceramic pillars from level I to level IV is 8, 4, 2, and 1 mm, respectively.

2) 3-D printer (Pico Plus 27, ASIGA, USA) was used to manufacture a mold to represent the negative of the SG fractal geometry, which is shown in Fig. 12(b), for the function of holding the ceramic pillars in position.
3) The ceramic pillars were placed in the mold, shown in Fig. 12(c) and filled with RX771C(NC)/CY1300 hard-set epoxy polymer (Robnor Resin Ltd., Swindon, U.K.), as shown in Fig. 12(d).
4) Once the polymer filler was fully cured, the mold was machined OFF and the composite plate was lapped down to the desired thickness 2.6 mm. The prototype of this SG fractal composite is shown in Fig. 12(e) and is the first manufactured piezoelectric device based on fractal theory.

An equivalent conventional parallelepiped 1–3 composite was also fabricated using the traditional dice-and-fill technique, in order to compare performance. For each device a dual matching layer was employed, the design of which is described in Section III-B2). Finally, each device was secured into a water proof housing. Fig. 13 shows a photograph of the complete SG fractal piezoelectric composite transducer (left) and an equivalent conventional composite (right) together with a £1 coin (middle) which has a diameter of 25 mm.

V. Experimental Validation

The performance of the manufactured SG fractal composite transducer was characterized experimentally in three different modes: one-way transmission, one-way reception, and two-way pulse-echo. The measured TVR, OCV, and the pulse-echo response of the SG fractal composite device are compared with the equivalent conventional composite design and an unfocused commercial ultrasound transducer (A301 S, Panametrics, USA). The specifications of three devices are stated in Table IV.

Fig. 13. SG fractal (left) and conventional composite (right) ultrasonic transducer.

TABLE IV
Transducer Specification

	Pulse-Echo Centre Frequency	Active Aperture Area
SG Fractal Device	596 kHz	131.9 mm^2
Conventional Device	587 kHz	123.2 mm^2
Panamterics Commercial Device	547 kHz	615.7 mm^2

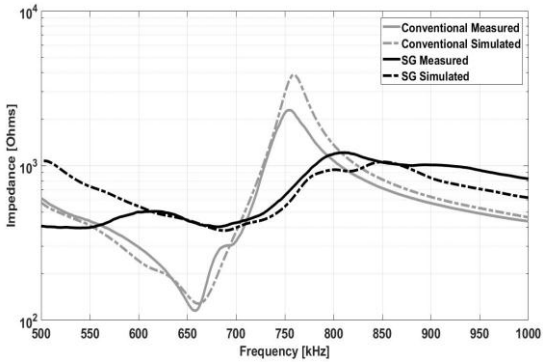

Fig. 14. Simulated and measured impedance.

It should be noticed that the commercial device has a much larger active area compared with the two fabricated devices: this significant active area difference will be taken into account in the experimental results comparison between these three devices.

A. Impedance Response of Fabricated Devices

The electrical impedance responses of the fabricated devices with matching layers casted were measured in air and they correlate well with the simulation results, as shown in Fig. 14. The k_t was measured as 0.54 and 0.50 for the SG fractal and conventional composite, respectively, and the relative dielectric constants ε_r of both devices using the constant strain condition are calculated as 706 and 986 for the SG and conventional composite, respectively.

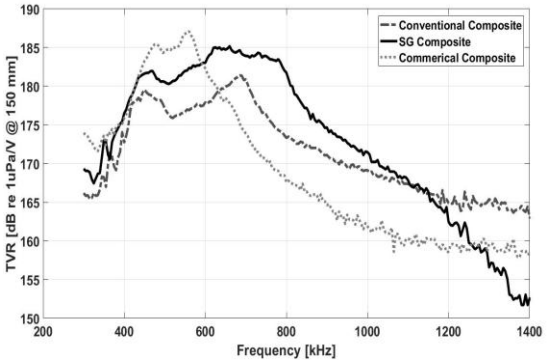

Fig. 15. Measured TVR spectrum of the three ultrasonic transducers.

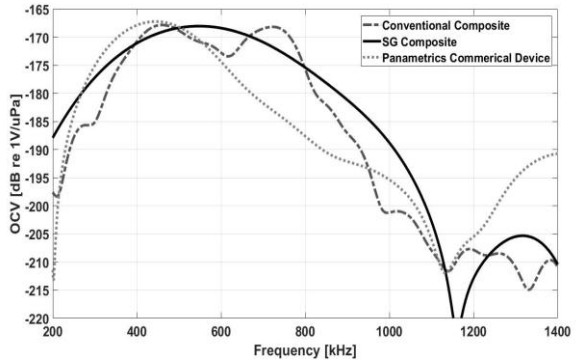

Fig. 16. Measured OCV spectrum of the three ultrasonic transducers.

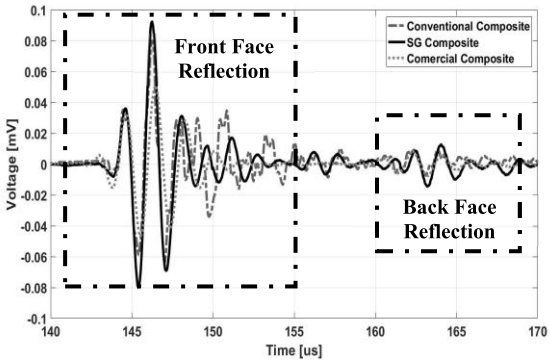

Fig. 17. Measured time-domain pulse-echo waveform.

B. Transmission Response Measurement

For characterizing the performance of the devices in transmission mode, the TVR of these three devices was measured experimentally. A function generator (33210A, KEYSIGHT, USA) was used to excite each testing transducer with a 20 cycles tone burst sine signal and the frequency of the tone burst signal varied from 300 to 1500 kHz with the step of the 5 kHz. A calibrated hydrophone (IP-124, GEC Marconi Ltd., U.K.) is located in the far field of the transducer (150 mm away from the transducer front face) for capturing the transmitted signal. The input and received signal was displayed using an oscilloscope in the time domain. The TVR in frequency domain was obtained using (9).

The TVR spectra of the three devices are shown in Fig. 15. The -6-dB transmitting operational bandwidth of these devices is calculated as 64.0% for the SG fractal device, 50.3% for the equivalent conventional composite design, and 31.2% for commercial transducer. This equates to a 27.2% and 105.1% bandwidth improvement by the SG fractal device. In terms of the sensitivity level, the peak gain of the SG fractal device is 3.8-dB higher than the conventional composite design. However, the peak gain of the SG fractal device is 1.9-dB lower when compared to the commercial transducer, which is due to the significant difference in active aperture areas of each device.

C. Reception Response Measurement

In order to test the performance of the SG fractal device in reception mode, a broadband $9-\mu$m customized polyvinylidene fluoride (PVDF) transducer was used as a transmitter for generating a common acoustic signal and a calibrated hydrophone was initially used as the reference receiver. The field pressure characteristic generated by the PVDF transmitter was measured by the calibrated hydrophone first. Once a calibrated reference signal was recorded, the PVDF transmitter was replaced by each of the three devices and the field pressure measured. The distance between the reference hydrophone and the receiving device was maintained at 150 mm. The OCV response can be calculated using (10), and the resulting measured spectra are shown in Fig. 16.

In Fig. 16, it can be seen that the -6-dB receiving bandwidth of the SG fractal device, the conventional composite design, and the commercial transducer are 78.8%, 76.9%, and 59.3%, respectively, resulting in a 2.5% and 32.9% bandwidth extension being realized by the SG fractal design. It should be noted that because commercial device has a larger active aperture area, the peak again of the commercial device is higher than both SG fractal design and conventional device.

D. Pulse-Echo Response Measurement

In order to further validate the advantage of designing a composite ultrasound transducer using a fractal geometry, the pulse-echo response of each device was measured experimentally. The transducer was positioned in the water tank and a flat glass reflector with thickness of 50 mm was placed in the far field of the transducer, which is 100 mm away from the transducer front face. The pulser/receiver (5052 PR, Panametrics, USA) was used to excite each transducer and then receive the reflected echo signal. The received echo signal was amplified with a gain of 20 dB by the pulser/receiver and displayed using an oscilloscope. Because the active aperture area is different between these three devices, the measured time domain waveforms were normalized with respect to the transducer active area and are shown in Fig. 17. The resulting frequency responses are shown in Fig. 18.

The resulting peak-to-peak echo signals from the front and back faces of the glass reflector in Fig. 17 and the -6-dB fractional bandwidths for the three devices calculated from Fig. 18 are shown in Table V.

In the two-way pulse-echo experimental setup, the SG fractal device displayed an improved signal strength compared to the other devices. When the received time domain echo signal is normalized with respect to the transducer active aperture area, the signal strength of the SG fractal design is

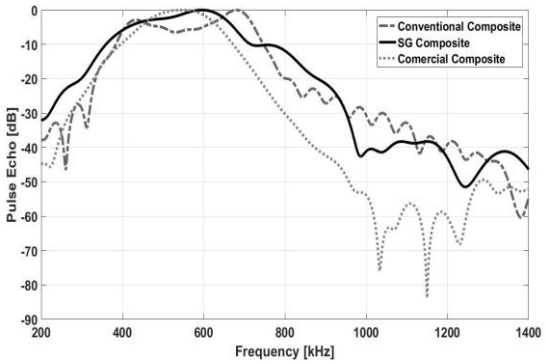

Fig. 18. Pulse-echo frequency response spectra.

TABLE V
PULSE-ECHO EXPERIMENTAL RESULTS

	Front Face Echo	Back Face Echo	- 6dB Bandwidth
SG Composite	0.17 mV	0.027 mV	47.5 %
Conventional Composite	0.14 mV	0.014 mV	47.8 %
Panametrics Commercial Device	0.10 mV	0.016 mV	38.9 %

increased by 21.4% and 70.0% with respect to the conventional composite and commercial devices, respectively. The −6-dB bandwidth of the SG fractal design is approximately the same as the conventional composite design but enhanced by 22.1% when compared with the commercial transducer.

VI. DISCUSSION AND CONCLUSION

This paper describes the implementation of the SG fractal geometry as the structure of a piezocomposite design in order to improve the transducer operational bandwidth. A finite element analysis simulation tool was used to build a 3-D SG fractal composite transducer model for the purpose of predicting its behavior and comparing with an equivalent conventional composite design. The simulation results showed that when applying the SG fractal geometry at fractal generation levels greater than level III; a wider bandwidth can be achieved in both transmission and reception modes compared to an equivalent conventional design.

As a result, the decision to manufacture a prototype SG fractal composite transducer at level IV was made using the pillar placement method, where the ceramic pillars in different sizes were positioned individually in a 3-D printed mold. An equivalent conventional composite device was manufactured using the traditionally dice-and-fill technique for the purpose of comparison. In order to validate the simulation results, the performance of this SG fractal transducer was characterized in three different configurations: one-way transmission mode, one-way reception mode, and two-way pulse-echo mode. The experimental results were compared with the manufactured conventional composite transducer and a commercial Panametrics transducer. The experimental results correlate well with the simulation results. First of all, the SG fractal device exhibits a wider bandwidth and higher sensitivity characteristic in transmission mode compared to the conventional composite design and commercial device. Second, in the reception mode, the SG fractal device can operate in a broad frequency range but has a lower sensitivity when compared with the other two devices. Finally, in the pulse-echo experiment, the SG fractal design shows an encouraging improvement with regards to the signal strength compared to both conventional devices and a bandwidth enhancement when compared to the commercial device.

It should be noted that in this work neither of the 1–3 composite or SG fractal devices has been backed, whereas the commercial device incorporates both matching and backing to extend bandwidth. Therefore, the device comparison is not direct, with the commercial device used to provide a known benchmark performance against which the other devices can be compared. This is particularly evident in Fig. 17, where the axial resolution of the commercial device would highlight this device for conventional imaging applications. Similarly, the pseudorandom composite, as developed by Yang *et al.* [20], incorporates both matching and backing layers has a measured −6-dB pulse-echo bandwidth of 61%, whereas the unbacked fractal composite in this paper has a measured −6-dB pulse-echo bandwidth of 47.5%. Nevertheless, the SG device has achieved a wider operational bandwidth compared to the equivalent standard 1–3 composite and hence, the addition of a backing layer in the future designs should provide additional damping to improve the axial resolution performance and increase the operational bandwidth.

There are two main challenges in manufacturing this SG fractal device due to the limitation of the 3-D printing and ceramic dicing technique, which would have effect on the composite performance. First of all, the mold needs to be designed carefully and 3-D printed precisely in order to make sure the individual pillars can be placed accurately into the mold and importantly, they must also stay in a vertical position during the remainder of the fabrication process. Second, it is difficult to cut triangular in small sizes and time consuming to manually place small sized pillars into the mold. As the results, there is a possibility that pillars may not stand vertically in the 3-D printed mold, which might cause some negative influence on the transducer's performance. For example, according to the experimental results, the SG composite still exhibits an improved bandwidth in reception and pulse-echo modes when compared to the conventional composite, but the improvement is no longer as apparent as what was predicted in the simulation results. Due to these manufacturing limitations, it would be very difficult and time consuming to manufacture this kind of SG fractal device in a higher fractal generation level or at a higher operating frequency range (above 1 MHz). However, one reason that the self-similar fractal geometry would still be a valuable choice compared with a random distributed geometry is that the fractal geometry can be generated by the following a simple algebraic rule, which facilitates analyses of the transducer performance within the design space.

Future SG fractal transducer designs should consider higher generation levels operating at frequencies above 1 MHz, which will lead to a finer composite microstructure. This will not only offer the potential to introduce a further extension of the

operating bandwidth across a wider range of applications, but also reduce the pillar aspect ratio of the triangular pillars in higher generation levels, which will result in a reduction of the antiphase behavior and an enhancement of the surface dilation quality of the device. To achieve this, the use of more advanced fabrication techniques will be required. Two potential solutions that could be considered are: 3-D printing of the piezoelectric ceramic microstructure [34] or using a programed laser cutting technique to machine the bulk ceramic [35].

In summary, based on the evidence from the FE simulation and experimental results shown in this paper, the operational performance of a piezoelectric composite ultrasonic transducer can be improved by using a fractal geometry as the microstructure of active layer. This is due to the multiscale active elements within the fractal composite structure.

ACKNOWLEDGMENT

The authors would like to thank the staff and researchers of the Centre for Ultrasonic Engineering, University of Strathclyde, Glasgow, U.K., for all the support throughout this research work. The research data associated with this paper are available at http://dx.doi.org/10.15129/7cdfd277-2091-4b50-b073-0b039d1b83f1.

REFERENCES

[1] R. E. Newnham, D. P. Skinner, and L. E. Cross, "Connectivity and piezoelectric-pyroelectric composites," *Mater. Res. Bull.*, vol. 13, no. 5, pp. 525–536, May 1978.

[2] T. R. Gururaja *et al.*, "Composite piezoelectric transducers," in *Proc. IEEE Ultrason. Symp.*, Nov. 1980, vol. 53, no. 9, pp. 576–581.

[3] G. Hayward and J. Bennett, "Assessing the influence of pillar aspect ratio on the behavior of 1–3 connectivity composite transducers," *IEEE Trans. Ultrason., Ferroelectr., Freq. Control*, vol. 43, no. 1, pp. 98–108, Jan. 1996.

[4] J. Bennett and G. Hayward, "Design of 1–3 piezocomposite hydrophones using finite element analysis," *IEEE Trans. Ultrason., Ferroelectr., Freq. Control*, vol. 44, no. 3, pp. 565–574, May 1997.

[5] K. C. Benjamin, "Recent advances in 1–3 piezoelectric polymer composite transducer technology for AUV/UUV acoustic imaging applications," *J. Electroceram.*, vol. 8, no. 2, pp. 145–154, 2002.

[6] S. Cochran, M. Parker, and P. Marin-Franch, "Ultrabroadband single crystal composite transducers for underwater ultrasound," in *Proc. IEEE Ultrason. Symp.*, vol. 1, Sep. 2005, pp. 231–234.

[7] P. Marin-Franch, I. Pettigrew, M. Parker, K. J. Kirk, and S. Cochran, "Piezocrystal-polymer composites: New materials for transducers for ultrasonic NDT," *Insight Non-Destruct. Test. Condition Monit.*, vol. 46, no. 11, pp. 653–657, 2004.

[8] E. S. Ebbini, C. Simon, H. Lee, and W. Choi, "Self-guided ultrasound phased arrays for noninvasive surgery," in *Proc. IEEE Ultrason. Symp., Int. Symp.*, vol. 2, Oct. 1999, pp. 1427–1430.

[9] W. Hackenberger, X. Jiang, P. Rehrig, X. Geng, A. Winder, and F. Forsberg, "Broad band single crystal transducer for contrast agent harmonic imaging," in *Proc. IEEE Symp. Ultrason.*, Oct. 2003, pp. 778–781.

[10] A. Rodríguez *et al.*, "Split Spectrum processing applications for new composite materials imaging," in *Proc. IEEE Int. Ultrason. Symp.*, Oct. 2012, pp. 1473–1476.

[11] J. Saniie, E. Oruklu, and S. Yoon, "System-on-chip design for ultrasonic target detection using split-spectrum processing and neural networks," *IEEE Trans. Ultrason., Ferroelectr., Freq. Control*, vol. 59, no. 7, pp. 1354–1368, Jul. 2012.

[12] K. Yamada, D. Yamazaki, and K. Nakamura, "Broadband ultrasound transducers using a plate with a graded piezoelectric constant formed by an internal temperature gradient," in *Proc. IEEE Ultrason. Symp.*, Oct. 2000, pp. 1017–1020.

[13] C.-M. Wong, Y. Chen, H. Luo, J. Dai, K.-H. Lam, and H. L.-W. Chan, "Development of a 20-MHz wide-bandwidth PMN-PT single crystal phased-array ultrasound transducer," *Ultrasonics*, vol. 73, pp. 181–186, Jan. 2017.

[14] J. A. Hossack and B. A. Auld, "Multiple layer transducers for broadband applications," in *Proc. IEEE Ultrason. Symp.*, 1991, pp. 605–610.

[15] G. Harvey, A. Gachagan, J. W. MacKersie, T. McCunnie, and R. Banks, "Flexible ultrasonic transducers incorporating piezoelectric fibres," *IEEE Trans. Ultrason., Ferroelectr., Freq. Control*, vol. 56, no. 9, pp. 1999–2009, Sep. 2009.

[16] S. N. Ramadas, R. L. O'Leary, A. Gachagan, G. Hayward, and R. Banks, "A wideband annular piezoelectric composite transducer configuration with a graded active layer profile," in *Proc. IEEE Int. Ultrason. Symp.*, Sep. 2009, pp. 2742–2745.

[17] R. Banks, R. L. O'Leary, and G. Hayward, "Enhancing the bandwidth of piezoelectric composite transducers for air-coupled non-destructive evaluation," *Ultrasonics*, vol. 75, pp. 132–144, Mar. 2017.

[18] F. M. de Espinosa, O. Martíez, L. E. Segura, and L. Gomez-Ullate, "Double frequency piezoelectric transducer design for harmonic imaging purposes in NDT," *IEEE Trans. Ultrason., Ferroelectr., Freq. Control*, vol. 52, no. 6, pp. 980–986, Jun. 2005.

[19] H. Guo, J. M. Cannata, Q. Zhou, and K. K. Shung, "Design and fabrication of broadband graded ultrasonic transducers with rectangular kerfs," *IEEE Trans. Ultrason., Ferroelectr., Freq. Control*, vol. 52, no. 11, pp. 2096–2102, Nov. 2005.

[20] H.-C. Yang, J. Cannata, J. Williams, and K. K. Shung, "Crosstalk reduction for high-frequency linear-array ultrasound transducers using 1–3 piezocomposites with pseudo-random pillars," *IEEE Trans. Ultrason., Ferroelectr., Freq. Control*, vol. 59, no. 10, pp. 2312–2321, Oct. 2012.

[21] W. Rössler, "Postembryonic development of the complex tibial organ in the foreleg of the bushcricket *Ephippiger ephippiger* (Orthoptera, Tettigoniidae)," *Cell Tissue Res.*, vol. 269, no. 3, pp. 505–514, 1992.

[22] W. Rössler, "Functional morphology and development of tibial organs in the legs I, II and III of the bushcricket *Ephippiger ephippiger* (Insecta, Ensifera)," *Zoomorphology*, vol. 112, no. 3, pp. 181–188, Sep. 1992.

[23] W. Rössler, A. Hübschen, J. Schul, and K. Kalmring, "Functional morphology of bushcricket ears: Comparison between two species belonging to the Phaneropterinae and Decticinae (Insecta, Ensifera)," *Zoomorphology*, vol. 114, no. 1, pp. 39–46, Mar. 1994.

[24] E. A. Algehyne and A. J. Mulholland, "A finite element approach to modelling fractal ultrasonic transducers," *IMA J. Appl. Math.*, vol. 80, no. 6, pp. 1684–1702, 2015.

[25] L.-A. Orr, A. J. Mulholland, R. L. O'Leary, and G. Hayward, "Analysis of ultrasonic transducers with fractal architecture," *Fractals*, vol. 16, no. 4, pp. 333–349, 2008.

[26] A. J. Mulholland and A. J. Walker, "Piezoelectric ultrasonic transducers with fractal geometry," *Fractals*, vol. 19, no. 4, pp. 469–479, 2011.

[27] J. A. Hossack and G. Hayward, "Finite-element analysis of 1–3 composite transducers," *IEEE Trans. Ultrason., Ferroelectr., Freq. Control*, vol. 38, no. 6, pp. 618–629, Nov. 1991.

[28] W. A. Smith and B. A. Auld, "Modeling 1–3 composite piezoelectrics: Thickness-mode oscillations," *IEEE Trans. Ultrason., Ferroelectr., Freq. Control*, vol. 38, no. 1, pp. 40–47, Jan. 1991.

[29] R. Lerch, "Simulation of piezoelectric devices by two- and three-dimensional finite elements," *IEEE Trans. Ultrason., Ferroelectr., Freq. Control*, vol. 37, no. 3, pp. 233–247, May 1990.

[30] D. Callens, C. Bruneel, and J. Assaad, "Matching ultrasonic transducer using two matching layers where one of them is glue," *NDTE Int.*, vol. 37, pp. 591–596, Dec. 2004.

[31] R. Hill and S. M. A. El-Dardiry, "A theory for optimization in the use of acoustic emission transducers," *J. Acoust. Soc. Amer.*, vol. 67, no. 2, p. 673, 1980.

[32] Q. Zhou, K. H. Lam, H. Zheng, W. Qiu, and K. K. Shung, "Piezoelectric single crystal ultrasonic transducers for biomedical applications," *Prog. Mater. Sci.*, vol. 66, pp. 87–111, Jun. 2014.

[33] R. L. O'leary, G. Hayward, G. Smillie, and A. C. S. Parr, "CUE materials database," Centre Ultrason. Eng., Glasgow, U.K., Version 1, 2005.

[34] Z. Chen *et al.*, "3D printing of piezoelectric element for energy focusing and ultrasonic sensing," *Nano Energy*, vol. 27, pp. 78–86, Sep. 2016.

[35] K. Li, D. W. Zeng, K. C. Yung, H. L. W. Chan, and C. L. Choy, "Study on ceramic/polymer composite fabricated by laser cutting," *Mater. Chem. Phys.*, vol. 75, nos. 1–3, pp. 147–150, Apr. 2002.

Haoyu Fang (GS'16–M'17) was born in Lanzhou, China, in 1991. He received the B.S. degree in electronic and electrical engineering from the University of Strathclyde, Glasgow, U.K., in 2014, where he is currently pursuing the Ph.D. degree with the Center for Ultrasonic Engineering.

His research interests include nature-inspired ultrasound and broadband ultrasound transducer design.

Zhen Qiu (S'10–M'13) received the B.Eng. degree in measuring and control technology and instruments from Tianjin University, Tianjin, China, in 2007, and the M.Sc. degree in biomedical engineering and the Ph.D. degree in electronic engineering and physics from the University of Dundee, Dundee, U.K., in 2009 and 2014, respectively.

She was with the Institute for Medical Science and Technology, University of Dundee, where she was involved in medical ultrasound. In 2014, she joined the Centre for Ultrasonic Engineering, University of Strathclyde, Glasgow, U.K. Her research interests include new piezoelectric materials and piezocrystals, and their adoption to improve performance transducer arrays for a range of applications, such as ultrasound surgery, ultrasound-targeted drug delivery, microultrasound diagnostic imaging, underwater sonar, and nondestructive testing.

Anthony J. Mulholland was born in Glasgow, Scotland, U.K., in 1966. He received the B.Sc. Honours degree in mathematics from the University of Glasgow, Glasgow, in 1987, the M.Sc. degree in industrial mathematics from the University of Strathclyde, Glasgow, in 1991, and the Ph.D. degree in mathematical biology from Glasgow Caledonian University, Glasgow, in 1994.

Since 1996, he has been with the Center for Ultrasonic Engineering, University of Strathclyde, where he currently leads the analytical modeling activities of the center. Since 1999, he has been an academic Staff Member with the Department of Mathematics and Statistics, University of Strathclyde, where he is currently a Professor and the Head of the Department. He has authored or coauthored over 100 papers in applied mathematics, particularly in the modeling of ultrasonic devices and systems.

Dr. Mulholland is a fellow of the Institute of Mathematics and its Applications.

Richard L. O'Leary (A'06–M'10) received the Ph.D. degree from the University of Strathclyde, Glasgow, U.K., focusing on passive polymer phase of piezoelectric composite transducers.

He is currently a Lecturer with the Centre for Ultrasonic Engineering, Department of Electronic and Electrical Engineering, University of Strathclyde. His research interests include the application of novel polymer systems to both piezoelectric and capacitive transducers and arrays, materials characterization, finite-element modeling, multilayered devices, and the application of ultrasound to nondestructive evaluation.

Anthony Gachagan (M'04) received the Ph.D. degree from the University of Strathclyde, Glasgow, U.K., in 1996, focusing on the development of air-coupled piezoelectric transducer technology and has continued to develop his ultrasonic transduction research into array technology and high power system.

He is currently a Professor with the Department of Electrical and Electronic Engineering, Strathclyde University, where he is also the Director of the Centre for Ultrasonic Engineering. He focused on the field of ultrasound for over 25 years. He has authored or coauthored over 120 research publications across a broad application range including nondestructive evaluation, sonar, bioacoustics, and industrial process control. His research interests encompass ultrasonic transducers and arrays, array imaging processing, power ultrasound, industrial process control instrumentation, and the application of coded excitation techniques.